Noncontact Dipole Effects on Channel Permeation. I. Experiments with (5F-Indole)Trp[13] Gramicidin A Channels

David D. Busath,* Craig D. Thulin,* Richard W. Hendershot,* L. Revell Phillips,* Peter Maughan,* Chad D. Cole,* Nathan C. Bingham,* Sara Morrison,* Lissa C. Baird,* Reed J. Hendershot,* Myriam Cotten,# and Timothy A. Cross#

*Zoology Department, Brigham Young University, Provo, Utah 84062, and #Center for Interdisciplinary Magnetic Resonance at the National High Magnetic Field Laboratory, Institute of Molecular Biophysics and Department of Chemistry, Florida State University, Tallahassee, Florida 32306 USA

ABSTRACT Gramicidin A (gA), with four Trp residues per monomer, has an increased conductance compared to its Phe replacement analogs. When the dipole moment of the Trp[13] side chain is increased by fluorination at indole position 5 (FgA), the conductance is expected to increase further. gA and FgA conductances to Na^+, K^+, and H^+ were measured in planar diphytanoylphosphatidylcholine (DPhPC) or glycerylmonoolein (GMO) bilayers. In DPhPC bilayers, Na^+ and K^+ conductances increased upon fluorination, whereas in GMO they decreased. The low ratio in the monoglyceride bilayer was not reversed in GMO-ether bilayers, solvent-inflated or -deflated bilayers, or variable fatty acid chain monoglyceride bilayers. In both GMO and DPhPC bilayers, fluorination decreased conductance to H^+ but increased conductance in the mixed solution, 1 M KCl at pH 2.0, where K^+ dominates conduction. Eadie-Hofstee plot slopes suggest similar destabilization of K^+ binding in both lipids. Channel lifetimes were not affected by fluorination in either lipid. These observations indicate that fluorination does not change the rotameric conformation of the side chain. The expected difference in the rate-limiting step for transport through channels in the two bilayers qualitatively explains all of the above trends.

INTRODUCTION

The recent publication of the *Streptomyces lividans* potassium channel structure (Doyle et al., 1998) allows for the understanding of some of the general features of ion flow in the voltage-gated channel superfamily. Evaluation of the potential of mean force for moving an ion through a channel is mainly an electrostatic problem. This problem can be subdivided into three types of ion-environment interactions: short-range interactions between the ion and adjacent atoms in protein side chains, backbone, and water; middle-range interactions with more distant residues and noncontact pore waters; and long-range interactions with lipid and bulk water. Because this appears to be a simple breakdown, it is tempting to ignore the long- and middle-range interactions, but the anisotropy of the lipid membrane system and the potential for the multipoles, comprising the ion and adjacent charges, to produce very large interactions with middle- and long-range structures require their full inclusion in any permeation model. The gramicidin channel is ideal for the development of mesoscopic and microscopic theories for these three scales of interactions because it is small, yet analysis of channel conductivity depends heavily on all three elements. Progress in evaluating the role of these three types of interactions in governing gramicidin channel permeability has been under way for some time (e.g., Andersen, 1983; Jordan, 1984).

Gramicidin A is a 15-amino acid peptide that dimerizes head-to-head to form cation-selective channels (Busath, 1993; Andersen and Koeppe, 1992; Woolley and Wallace, 1992). The secondary structure consists of a single-stranded $\beta^{6.5}$-helix. The cylindrical structure of gA is held together by β-pleated-sheet hydrogen bonds, as in the common β-barrels composed of 6–20 or more strands (Branden and Tooze, 1991), the single-stranded β-helical pectate lyase (Yoder et al., 1993), and a recently proposed set of double-stranded β-helix structures for amyloid fibrils (Lazo and Downing, 1998). D-Chirality of the even-numbered residues in gA allows all side chains to project away from the lumen of the helix, yielding a tight wind (6.5 amino acids per turn) with a patent channel, in contrast to proteins formed from all L amino acids. The high-resolution structure in multilayers has recently been published (PDB accession number 1MAG; Ketchem et al., 1997).

This report is the first in a series designed to focus on the role of middle-range interactions controlling ion flow through gramicidin channels. Direct contacts with peptide backbone (e.g., Roux and Karplus, 1993) and pore waters (e.g., Partenskii et al., 1991) have been analyzed theoretically but are not accessible to experimental variation, except at the channel termini (e.g., Roeske et al., 1989). The peptide side chains in gramicidin, however, project away from the channel. Changes in the electrostatic configuration of the side chains are expected to modify the electric field in the channel through space by way of their multipole moment. This has been shown to be the case with fluorinated valine side chains (Koeppe et al., 1990), where the role of

Received for publication 9 June 1998 and in final form 26 August 1998.

Address reprint requests to Dr. David Busath, Zoology Department, Brigham Young University, Provo, UT 84602. Tel.: 801-378-8753; Fax: 801-378-7423; E-mail: david_busath@byu.edu.

Dr. Thulin's present address is Department of Chemistry and Biochemistry, Brigham Young University, Provo, UT 84602.

0006-3495/98/12/2830/15 $2.00

inductive effects on backbone atoms in direct contact with permeating cations was discounted. Interactions between permeating ions and gA side chains are therefore representative of the middle-range interactions expected in larger protein channels.

In gramicidin channels, Trps at positions 9, 11, 13, and 15 are located near the bilayer surface (Busath, 1993). They have significant axial dipole moments and thus modulate the conductance of permeating cations. These Trps have been shown to enhance conductance compared to phenylalanine or other nonpolar side chains (Bamberg et al., 1976; Heitz et al., 1982, 1986, 1988; Daumas et al., 1989, 1991; Becker et al., 1991; Fonseca et al., 1992; Seoh and Busath, 1995). In each case, replacement of a Trp with a nonpolar side chain or modification of the Trp indole to reduce the dipole moment resulted in a decrease in alkali metal conductance. Surface potentials in dioleoylphosphatidylcholine (DOPC) monolayers reflect the interfacial dipole potential, which comprises part of the translocation barrier (see below). The interfacial dipole potentials were reduced in gA-containing monolayers more than in monolayers containing a gA analog with all four Trps replaced with Phe (Heitz et al., 1989). The only exception to Trp enhancement of conductance reported so far is the observation, published only in abstract form (Sandblom et al., 1990), that in GMO bilayers proton conductance is lower in gA by ~25% compared to gramicidin B, the analog of gA in which Trp^{11} is replaced by Phe.

Sancho and Martínez (1991; see also Martínez and Sancho, 1993) have explained the effects of Trp dipoles on alkali metal cation conductance by using a continuum dielectric model in which the tryptophans are represented as a dipole annulus surrounding the channel entry and exit. They explored various dipole structures theoretically, including one in which the indole NH, the positive end of the indole dipole, projects out toward the water bath and the benzene (negative) end projects toward the center of the bilayer. The transport process is assumed to consist of electrodiffusion through a fairly featureless pore containing symmetrical binding sites of modest strength near the entry and exit and a broad, low-energy barrier to translocation between the sites due to long-range electrostatic forces. In the Sancho and Martínez model, the barrier in the center of the channel is reduced by the negative end of the annular dipole, which stabilizes a cation in the center of the channel. This stabilization is expected to enhance conductance to the extent that translocation from the entry site to the exit site is rate limiting. Because the bath electrolyte shields the positive end of the dipole annulus, inhibition of ion entry becomes less significant. Similar results have been obtained by computation of the Trp electrostatic potential of mean force (PMF) from molecular dynamics trajectories (Woolf and Roux, 1997). The anomalous result for proton conductance in gramicidin B remains unexplained.

The Trp side-chain conformations were explored initially by molecular modeling (Venkatachalam and Urry, 1983) and Raman spectroscopy studies (Takeuchi et al., 1990). These studies indicated a large number of possible conformation sets for the four Trps, but were not able to identify the primary conformation. The indole-NH out orientation was subsequently identified for all four Trp side chains when the specific side-chain dihedral angles were determined for gA embedded in dimyristoylphosphatidylcholine (DMPC) bilayers by solid-state NMR (Hu et al., 1993; see also Koeppe et al., 1994; Hu et al., 1995; and Ketchem et al., 1997). The solid-state NMR DMPC Trp conformations for all four Trp side chains are near the standard $\chi_1 = -60°$, $\chi_2 = -90°$ conformation. Hu and Cross (1995) pointed out that the Trp dipole projects toward a permeating cation when positioned at the center of the channel, which would stabilize the cation, consistent with the Sancho and Martínez (1991) analysis. The sum of the interaction energies between the zero to four dipoles (Trp side chains) and monopole (cation at the channel center) has been shown to correlate with the logarithm of the conductance for a series of Trp-to-Phe mutants for which the conductance has been measured (Becker et al., 1991).

Fluorination of indole position 5 increases the dipole moment measured at 30°C by a factor of 1.75 in benzene, and more in polar media (Weiler-Feilchenfeld et al., 1970). Whereas previous studies have focused on the effects of eliminating the Trp dipole, this study is designed to explore the consequences of increasing the dipole moment. One might expect further stabilization of cations in the channel center to continue increasing cation transport. However, at some point, the translocation barrier may be fully compensated by the side-chain dipoles, and increased dipole moments will not increase conductance. When this occurs, it may even be possible that the positive end of the dipole becomes inhibitory as entry becomes the rate-limiting process in transport.

Here we show that the effect of fluorination of Trp^{13} on gramicidin conductance differs markedly, depending on the type of lipid used. This could be due to fluorination-induced conformational differences between DPhPC and GMO bilayers. However, we present three lines of evidence indicating that any such conformational changes, if present, are minimal. As an alternative explanation, we suggest that the kinetics of ion transport vary between the two media. Eisenman et al. (1983) suggested that the variance in ion transport between the two types of lipid is due to the difference in interfacial dipole potentials. Using monolayer surface potential measurements and hydrophobic cation-anion conductivity differences, the interfacial potential has been estimated to differ between GMO and PC bilayers by ~120 mV (more positive in the bilayer interior for PC) (Hladky and Haydon, 1973; Pickar and Benz, 1978). The interfacial potential combines with the long-range ion-induced bulk water (image) potential and the middle-range peptide radial dipole potential to produce a broad barrier to translocation (Jordan, 1984). The difference in interfacial potentials is expected to increase the electrostatic energy at the center of the channel for alkali metal cations by ~1.5 kcal/mol in DPhPC bilayers when compared to GMO bilayers when the

shielding effects of the channel and lipid dielectrics (~50% reduction; Jordan, 1984) are taken into account. The interfacial dipole potential is not expected to affect ion entry because it does not extend into the bath, at least not sufficiently to affect hydration forces between closely packed bilayers (Gawrisch et al., 1992).

This paper represents the first report of a project designed to correlate fluorinated gramicidin conductance with information about the side-chain conformation from solid-state NMR. Our investigation reports the results of homodimer conductance measurements using standard conditions of ion concentration and species, lipid bilayer composition, and membrane potential. The effect of fluorination on channel conductance was found to depend on the lipid, ion, and voltage. Alkali metal cation conductance was anomalously inhibited in GMO bilayers, and hydronium conductance was inhibited in both GMO and DPhPC bilayers. We speculate about the possible interpretation of these results and their implications for other studies but reserve detailed structural and computational analysis for future work. Some of these results were reported in preliminary form (Thulin et al., 1998). Similar results have been reported for fluorinated gA analogs by Andersen et al. (1998) for DPhPC bilayers, but without analysis of GMO bilayer behavior or proton conductance effects.

MATERIALS AND METHODS

Salt solutions were made using distilled water purified to >18 MΩ-cm with a Barnstead NANOpure II system (VWR Scientific, San Francisco, CA). Potassium chloride (Mallinckrodt, Paris, KY) and sodium chloride (Fischer Biotech, Fairlawn, NJ) were baked at >500°C for at least 1 h before use. HCl (Fisher) was diluted from concentrate. Alkali metal solution concentrations were verified with a conductivity meter (Orion Model 126). GMO, glycerylmonoeicosenoin (GME), and glycerylmonopalmitolein (GMP) (NuChek Prep, Elysian, MN), GMO ether (Serdary Research Labs, ON, Canada), DOPC, DPhPC (Avanti Polar Lipids, Birmingham, AL), *n*-hexadecane, and *n*-decane (Aldrich, Milwaukee, WI) were used without additional purification. Squalene (Aldrich) was passed through an alumina (Aldrich) column and used within a day or two. All other lipid solutions were used for 2–4 weeks before discarding.

gA was purified from gramicidin D (ICN Nutritional Pharmaceuticals, Cleveland, OH) by high-performance liquid chromatography, using the method of Koeppe and Weiss (1981), and peptide solutions were prepared in methanol and diluted to 10^{-5} mg/ml. Original concentration was determined using an extinction coefficient of 22,600 M^{-1} cm^{-1} (Killian et al., 1987). FgA was synthesized by solid-phase synthesis using Fmoc (9-fluorenylmethoxycarbonyl) chemistry on an Applied Biosystems model 430A peptide synthesizer. Isotopically labeled d4-indole 5-fluoro L-tryptophan was purchased from Cambridge Isotope Laboratories (Woburn, MA). Details of the synthesis and blocking chemistry have been described previously (Fields et al., 1988, 1989). Typically 20–50-pg injections of either the gA or the FgA were added to the 1–2-ml bath.

Lipid bilayers were formed under two conditions. Experiments with GMO were performed using bilayers formed on the aperture (60–350 μm in diameter) of a polyethylene pipette inserted in a Teflon chamber (Busath and Szabo, 1988). GMO was dispersed directly in hexadecane (50 mg/ml) and was painted on the pipette aperture and allowed to thin spontaneously. DPhPC in decane (20 mg/ml) was prepared from a DPhPC chloroform (10 mg/ml) solution. After the evaporation of chloroform to a thin layer, decane was added, and the solution was sonicated. DPhPC bilayers were painted on the 150-μm aperture in a delrin cup (Warner Instrument Corp., Hamden, CT). For both lipids, bilayers were painted with a polyethylene spatula under UV-free illumination.

Membrane potentials were applied by way of Ag-AgCl electrodes. Membrane currents were measured using, in the case of DPhPC bilayers, a Warner BC-525C Bilayer Clamp or, in the case of GMO bilayers, a List EPC7 patch-clamp amplifier (List Medical, Darmstadt, Germany), taking care to use the low-gain headstage to avoid amplifier oscillations due to high bilayer capacitance. Control experiments demonstrated that the two amplifiers were calibrated identically, and the channel conductances and bilayer properties did not depend on either the type of chamber used or the amplifier or analysis procedures. For each experiment, data were low-pass-filtered with a cutoff frequency f_c = 100 Hz and collected continuously, usually for 10–30 min, after bilayer formation. Data were collected on a Macintosh computer with a NI-DAQ data acquisition board (National Instruments, Austin, TX) and IGOR Pro (Version 3.01; Wave Metrics, Lake Oswego, OR). Current transitions reflecting channel openings and closings were detected and analyzed with the computer programs TAC and TACfit (Version 2.5; Skalar Instruments, Seattle, WA). For low-level signals, additional digital filtering was applied with cutoffs as low as 30 Hz. Single-channel currents lasting less than $1/f_c$ were disregarded.

Because of dry climate, it was necessary to minimize evaporation from the saline bath. Evaporation was limited to 0.3–1.3%/h, measured gravimetrically, by keeping the solution within an enclosed Faraday cage, avoiding exposure of the solution to drafts, and swift bilayer formation. Conductance experiments were limited to ~30 min.

In a given experiment, single-channel currents primarily fit within a normal distribution. Low-conductance (mini) channels (Busath and Szabo, 1988) were ignored. Mean single-channel currents for each of at least three independent experiments were normalized to a 23°C room temperature, using Q_{20} = 1.9 (Hladky and Haydon, 1972) and then averaged, using the standard deviation of the fitted normal curve as a weighting factor. Temperature corrections rarely exceeded 2°C. If the standard deviation among experiments was unusually high (>0.1 pA), the experiment was repeated. The expected uncertainty in applied membrane potential was less than 0.3 mV because of possible drift in the electrode potentials. Bath concentrations were prepared with an accuracy of 0.1% and were verified by measuring conductivity.

The current ratio for the two compounds was computed from the population means for each of the two peptides:

$$R = \frac{i_{\mathrm{FgA}}}{i_{\mathrm{gA}}} \tag{1}$$

For n experiments with each peptide, the standard error of the population mean was computed from the standard deviation of the population, SD(i):

$$\mathrm{SEM}(i) = \frac{\mathrm{SD}(i)}{\sqrt{n}} \tag{2}$$

The standard error of the ratio, SE(R), was then calculated from the SEMs according to the method of propagation of errors (Bevington, 1969) as

$$\mathrm{SE}(R) = \frac{i_{\mathrm{FgA}}}{i_{\mathrm{gA}}}\sqrt{\frac{\mathrm{SEM}(i_{\mathrm{gA}})^2}{i_{\mathrm{gA}}^2} + \frac{\mathrm{SEM}(i_{\mathrm{FgA}})^2}{i_{\mathrm{FgA}}^2}} \tag{3}$$

We expected the accumulated errors to be less than 0.5% for well-controlled variables, including electrode potential drift, applied membrane potential, and prepared bath salt concentration. Interexperiment standard deviations were typically 2–3% of the conductance after temperature correction, presumably because of discrepancies from the nominal bath concentration and temperature. The accuracy of the measurements was calibrated by measuring the single-channel current for gA in 1 M KCl, V_m = 100 mV, in GMO bilayers (Urban, Hladky and Haydon, 1980) or in 1 M NaCl, V_m = 100 mV, in DPhPC bilayers (Russell et al., 1986). Values were routinely found to be within 2% of the previously reported results.

The linearity index (L.I.) for single-channel current-voltage relations is computed as

$$\text{L.I.} = \frac{2 \times g(200)}{(g(25) + g(50))} \quad (4)$$

where g is the conductance computed from the single-channel current, i, and the membrane potential, V_m:

$$g(V_m) = \frac{i}{V_m} \quad (5)$$

Average single-channel lifetimes were tabulated in a separate set of experiments for native and fluorinated gA in both GMO/hexadecane and DPhPC/decane bilayers, using lower peptide densities and $V_m = 100$ mV. Four experiments were carried out for each peptide in DPhPC bilayers, each with at least 745 channels; the average was 1675 channels. Five experiments were performed for each peptide in GMO bilayers, each with at least 260 channels; the average was 588 channels. Pre- and postexperiment air temperature was 26.0 ± 1.5°C for all DPhPC experiments and 24.5 ± 1.0°C for all GMO experiments; no temperature correction was performed for the lifetime measurements. To accommodate periods when multiple channels were conducting in parallel, the mean channel lifetime was determined from the equation

$$\tau = \frac{1}{N} \sum Ld \quad (6)$$

where a continuous current trace extending from one baseline segment to another is divided completely into constant-current segments of duration, d. $L = 0, 1, 2, \ldots$ is the number of channels conducting for each segment. The sum is over all of the flat data segments, ignoring any initial and terminal segments in which one or more channels were conducting. N is the number of channels, taken as the number of on (or off) transitions. The intraexperimental uncertainty in the mean (SEM), estimated for the exponential distribution as the mean divided by the square root of the total number of channels measured, was 0.006–0.02 s for DPhPC bilayers and 0.04–0.09 s for GMO bilayers. This was only a small component of the interexperimental standard deviation, reported in Table 3, which is presumably due to local and global temperature variations and variations in bilayer composition and structure.

Eadie-Hofstee plots were made by plotting the zero-current conductance (estimated as the conductance at 50 mV) against the same value divided by the permeant ion activity. Activity coefficients were taken from Moore (1972). For each combination of lipid bilayer type and permeant ion species, the data points at 0.1, 0.2, 0.5, and 1 M permeant ion were fitted to a straight line by the method of least squares.

RESULTS

Experiments with gA produced the typical unitary conductances with current-voltage-concentration relations similar to those previously published for DPhPC/decane and GMO/hexadecane bilayers (Becker et al., 1991; Busath and Szabo, 1988). FgA produced similar results in each case but differed in detail. We first display the results in DPhPC bilayers, comparing FgA to native gA. Then the results for GMO bilayers are presented, showing a marked contrast. Conductance behaviors in different bilayers illustrate the robust nature of the GMO anomaly. The effects of fluorination on hydronium conductance are then shown to be anomalous in both lipids. This leads to a more careful exploration of the current-voltage relation (*I-V*) shapes and Eadie-Hofstee plot behavior for gA and FgA in the two lipids. These results are integrated into a discussion of two models for the GMO anomaly presented in the Discussion.

Conductance properties in DPhPC bilayers

Fig. 1 shows single-channel currents in DPhPC bilayers for intermediate conditions (1 M salt, 100 mV) in NaCl and KCl for gA (*left*) and FgA (*right*). Other conditions of membrane potential and permeant ion concentration yield similar single-channel currents with no obvious change in single-channel noise or other properties.

Fig. 2 shows the *I-V*s for five ionic concentrations, in both KCl (*upper*) and NaCl (*lower*) baths for gA (*left*) and FgA (*right*) in DPhPC bilayers. Error bars reflect primarily the variation from experiment to experiment. The typical shift from sublinear at low concentrations to superlinear at high concentrations is seen for both gA and the fluorinated analog, but on careful examination it can be seen that the native peptide *I-V* is generally more superlinear for both ions.

In DPhPC, the ratio of FgA to gA conductance is greater than 1 under nearly all conditions. This is shown for Na^+ (Fig. 3 *a*) and for K^+ (Fig. 3 *b*), where the ratio is plotted as a function of membrane potential with symmetrical ionic bath concentration as a parameter. The ratio is greatest at the higher bath ion concentrations and at the lower applied potentials.

Conductance properties in GMO bilayers

In GMO bilayers, the single-channel currents were larger than in lecithin bilayers. Fig. 4 shows the single-channel currents in GMO bilayers for the same conditions as those in Fig. 1. Fig. 5 shows the *I-V* relations. It is evident in these two figures that in GMO bilayers FgA conductances are generally lower or approximately equal to gA conductances. This is borne out in the plot of current ratios in Fig. 6 (in sharp contrast to the enhancement of conductance produced

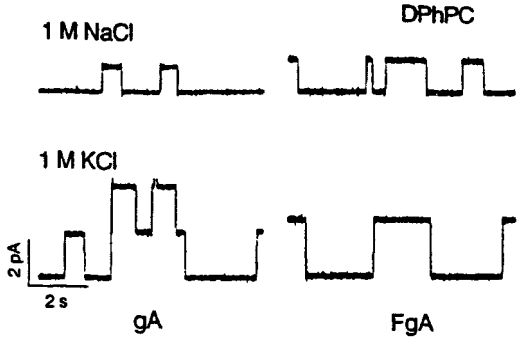

FIGURE 1 Single-channel currents for DPhPC bilayers at $V_m = 100$ mV are displayed for each of two bath ion species: 1 M Na^+ (*top*) and 1 M K^+ (*bottom*) for gA (*left column*) and FgA (*right column*). DPhPC/decane (20 mg/ml). Room temperature, 22–26°C.

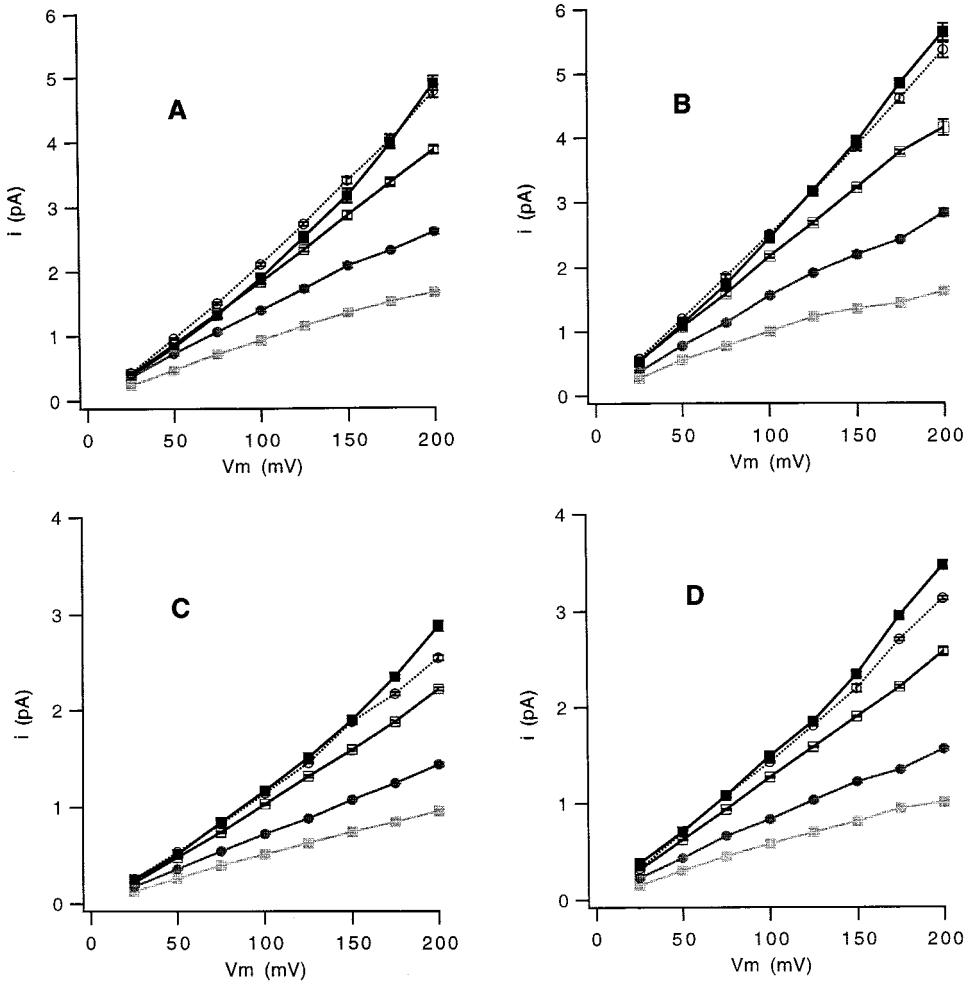

FIGURE 2 Single-channel current-voltage relationships in DPhPC, from bath solutions of KCl (*A*, *B*) and NaCl (*C*, *D*) for gramicidin A (*A*, *C*) and FgA (*B*, *D*). Currents increase with bath cation concentrations (except at 2.0 M), which were 0.1 (▨), 0.2 (●), 0.5 (□), 1.0 (○), and 2.0 M (■). Each point is the average of three or more experimental standard channel peak means. DPhPC/decane (20 mg/ml). Currents temperature corrected to 23°C. Error bars represent ± SEM of *i*.

by fluorination in DPhPC; see Fig. 3). For Na^+, fluorination has no discernible effect. For low concentrations of K^+, the ratio is below 1 at low voltages and rises toward 1 at high voltages. At the higher concentrations, the ratio exceeds 1. In GMO bilayers, the differences in the shapes of the *I-V*s are too subtle to discern in Fig. 5, but it is noteworthy that the current does not saturate with concentration at 2 M NaCl or 2 M KCl, as it does in DPhPC bilayers (Fig. 2).

Conductance properties in other bilayers

The conductance properties illustrated in Figs. 1–6 seem to be a feature of the headgroups rather than the bilayer interior. This is shown in Table 1, where gA and FgA conductances and their ratios are compared between bilayers differing in solvent inflation, acyl chain length, and headgroup structures. The use of different solvents with GMO pro-

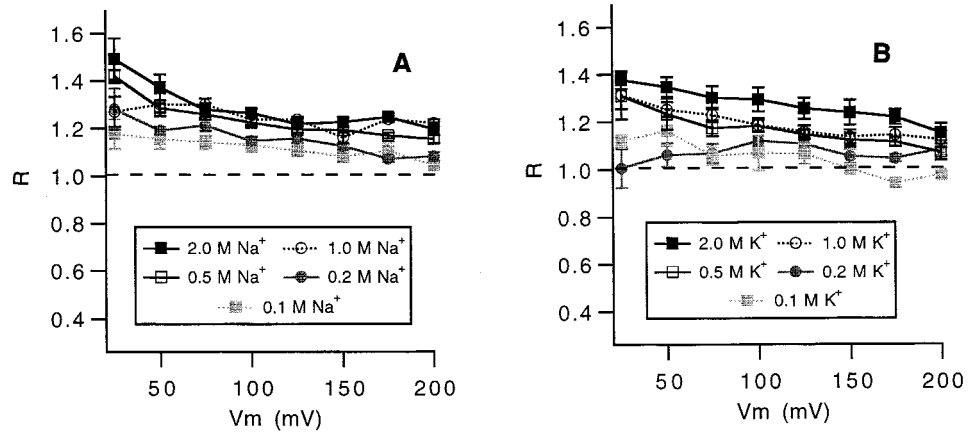

FIGURE 3 Ratio of temperature-corrected single-channel currents (fluorinated over native gA current) as a function of membrane potential for (*A*) Na^+ and (*B*) K^+. DPhPC/decane (20 mg/ml). Error bars represent ± SE of R.

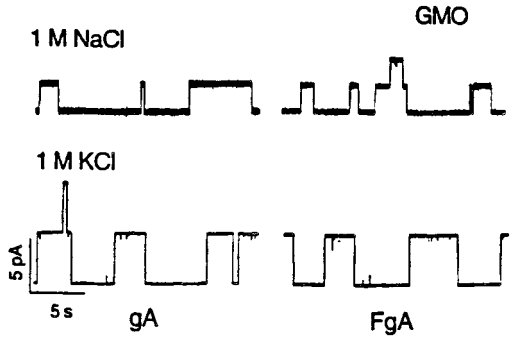

FIGURE 4 Single-channel currents for GMO bilayers at V_m = 100 mV are displayed for each of two bath ion species: 1 M Na^+ (*top*) and 1 M K^+ (*bottom*) for gramicidin A (*left column*) and FgA (*right column*). GMO/hexadecane (50 mg/ml). Room temperature, 22–26°C.

duces bilayers with hydrocarbon thicknesses of 25, 33, and 48 Å for squalene, hexadecane, and decane, respectively (Waldbillig and Szabo, 1979; Dilger, 1981). The different acyl chain lengths in GMP and GME yield bilayers of hydrocarbon thicknesses 29 Å and 39 Å, respectively, when inflated by hexadecane (Waldbillig and Szabo, 1979). The table shows that the drastic changes in bilayer thickness, whether by lengthening the acyl chain or by changing solvent inflation, did not alter the outcome of fluorination in monoglyceride bilayers. This is especially interesting in the case of GME bilayers in which the single-channel conductance is reduced quite markedly but equally for both peptides. Moreover, the conductances in GMO-ether differed little from those with the GMO ester. However, significant fluorination-induced enhancement of conductance is present in both types of PC bilayer.

Hydronium conductance properties

Interestingly, fluorination also produces an unexpected effect when H_3O^+ (hydronium) is the conducting species. Hydrogen-dependent currents are lower by ~15–25% in fluorinated peptides for both bilayer types in HCl at either pH 1 or pH 2 (Fig. 7, *lower traces*). Gramicidin channels and GMO headgroups have no titratable groups and tolerate high and low pH solutions well. DPhPC bilayers also tolerate pH changes. The titratable phosphate pK_a in bilayers is reduced by adjacent headgroup moieties to a level of $\sim<1$ (Marsh, 1990) but would still be likely to be partially protonated in solutions at pH 1. The single-channel current is much higher than for alkali metal cations at the same concentration because of Grotthus conductance (Hladky and Haydon, 1972). As a control for pH effects on the membrane surface or the Trp side chain in DPhPC bilayers, we

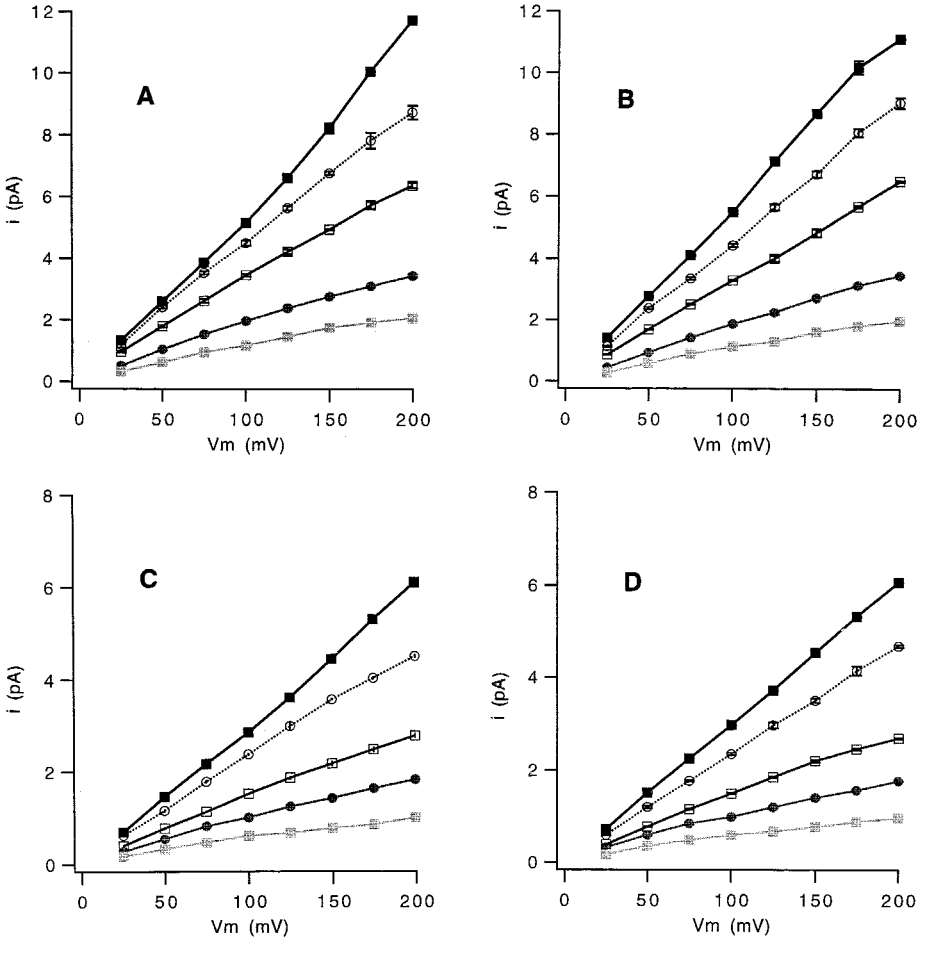

FIGURE 5 Single-channel current-voltage relationships in GMO using bath solutions of KCl (*A, B*) and NaCl (*C, D*) for gramicidin A (*A, C*) and FgA (*B, D*). Currents increase with bath cation concentrations, which were 0.1 (▨), 0.2 (●), 0.5 (□), 1.0 (○), and 2.0 M (■). Each point is the average of three or more experimental standard channel peak means. GMO/hexadecane (50 mg/ml). Currents temperature corrected to 23°C. Error bars represent ± SEM of *i*.

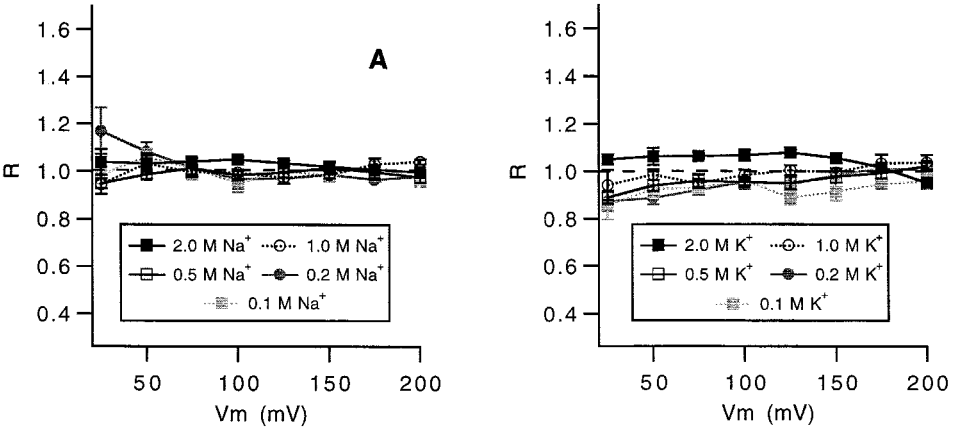

FIGURE 6 Ratio of temperature-corrected single-channel currents (fluorinated over native gA current) as a function of membrane potential for (*A*) Na^+ and (*B*) K^+. GMO/hexadecane (50 mg/ml). Error bars represent ± SE of R.

measured the conductance ratio in 1 M KCl at ~pH 2. Under these conditions, the majority of the current is carried by K^+, judging by the ratio of single-channel conductance at 100 mV in 1 M KCl (pH ~5.4) to that in 0.01 N HCl, which is 1.5 (i.e., 47 pS/32 pS). (This value represents an underestimate of the fraction of current carried by K^+, because the net current in the mixed solution (3.25 pA at 100 mV) was only 41% of the sum of the two currents for the two ions measured separately, indicating nonindependence of transport of the two ions. This is to be expected if K^+ is unusually effective in blocking Grotthus conductance, in which case the proportion of current carried by K^+ in the mixed solution could be much higher. However, we note that Na^+ was not found to block Grotthus conductance in a previous work (Heinemann and Sigworth, 1989).) The FgA/gA current ratio was 1.05–1.18 in DPhPC bilayers with 1 M KCl at pH 2 (Fig. 7, *triangles*), in contrast to the value of 0.77–0.87 when hydronium alone was the conducting species (Fig. 7, *solid squares*) in DPhPC at pH 2.

We next evaluate the impact of fluorination on the shapes of current-voltage and current-concentration relationships. In each case, we first introduce the interpretive framework usually employed with these types of data.

Current-voltage relation shapes

Shapes of the current-voltage (*I-V*) and current-concentration relation results have been used in the past to deduce the main steps of the transport mechanism, diffusion up to the channel and binding near the entry, translocation to the symmetrical exit site, and exit diffusion. *I-V* shapes are simply interpreted according to the voltage dependence of the rate-limiting step or process, following the approach used with carriers (e.g., Pickar and Benz, 1978) and utilized by others for gramicidin (Urban et al., 1978; Eisenman et al., 1983; Hägglund et al., 1984; Akeson and Deamer, 1991). (The free energy barriers to alkali metal cations are not dramatically different from each other and are not high, so that strictly speaking, the concept of a rate-limiting barrier as used in enzyme kinetics and interpretations based on Eyring rate theory models are not appropriate. Nevertheless, the patterns discussed here appear to be followed reasonably well for models appropriate to small broad barriers such as Brownian dynamics and Nernst-Planck or Poisson-Nernst-Planck, even though one particular barrier may not totally dominate the profile, and the concepts are conceptually simple. Therefore, we use the terms "energy barrier" and "rate-limiting step or process" throughout our descriptions for heuristic purposes, but point out that they are being used loosely and are not intended to imply a high barrier or Eyring rate theory paradigm.) In a permeation process in which a highly voltage-dependent step such as translocation is rate limiting, the *I-V* is superlinear. At low permeant ion concentrations, diffusion up to the channel entry becomes the rate-limiting process. There is little voltage drop in the bulk solution, so the *I-V* is sublinear. In principle, at high ion concentrations and high membrane potential, transport should become exit limited for ions with sufficient affinity for the channel (Akeson and Deamer, 1991), again producing a sublinear *I-V*, because exit, like entry, is not highly voltage dependent.

We start by noting the superlinearity of the *I-V*s in DPhPC bilayers (Fig. 2) compared with those in GMO bilayers (Fig. 5). Table 2 is a linearity index computed for each of the *I-V*s by dividing the 200-mV chord conductance by the average of 25 and 50 mV chord conductances. Linear *I-V*s have a linearity index of 1. The observed difference in linearity suggests that translocation is more rate limiting for DPhPC than GMO. In addition, there is more self-block in

TABLE 1 Lipid dependence of conductance

Lipid/solvent	gA current*	FgA current*	Ratio
GMO/squalene	4.53 ± 0.03	4.49 ± 0.02	0.99
GMO/hexadecane	4.49 ± 0.08	4.42 ± 0.06	0.98
GMO/decane	4.47 ± 0.07	4.39 ± 0.05	0.98
GMP/hexadecane	4.60 ± 0.05	4.65 ± 0.04	1.01
GME/hexadecane	3.88 ± 0.03	3.72 ± 0.02	0.96
GMO-ether/hexadecane	4.33 ± 0.08	4.48 ± 0.02	1.03
DOPC/decane	2.02 ± 0.03	2.55 ± 0.03	1.26
DPhPC/decane	2.11 ± 0.03	2.50 ± 0.04	1.18

*Currents (in pA ± SEM) were measured in 1 M KCl solution with a membrane potential of 100 mV.

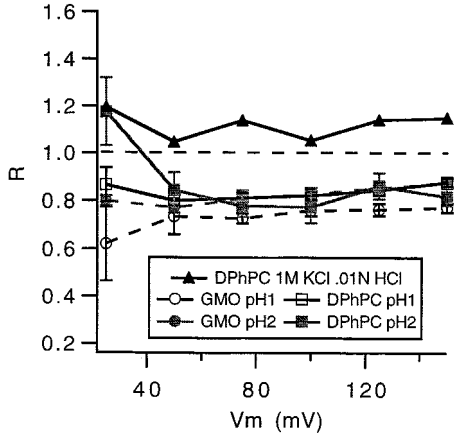

FIGURE 7 Ratio of temperature-corrected single-channel H^+ currents (fluorinated over native gA current) as a function of membrane potential, GMO/hexadecane (50 mg/ml) and DPhPC/decane (20 mg/ml). Temperature corrected to 23°C. Error bars represent ± SE of R.

DPhPC bilayers than in GMO bilayers. This can be seen in Fig. 2, where the 2 M *I-V* is below the 1 M *I-V*. Self-block is enhanced by translocation-limited transport (Hille and Schwarz, 1978; Hille, 1992). Furthermore, the transition from sublinear to superlinear occurs at a lower ion concentration in DPhPC bilayers (~0.2 M) than in GMO bilayers (1–2 M), as seen in Table 2. If, as an approximation, one supposes that the transition takes place at the concentration where the entry rate equals the translocation rate, this implies that in DPhPC bilayers the translocation step is more rate-limiting for any given concentration. These features all indicate that the barrier to translocation is more rate-limiting in DPhPC than in GMO.

Given this background, it is interesting to evaluate the effect of fluorination on *I-V* shape. Fig. 8 directly compares the *I-V*s of the two peptides in DPhPC bilayers with 0.5 M NaCl. The native peptide *I-V* is superlinear, whereas the fluorinated peptide *I-V* has a higher conductance and is essentially linear, consistent with a decreased barrier to translocation. This phenomenon is general for the other *I-V*s in DPhPC, as shown in Fig. 2 and summarized in Table 2. In GMO, on the other hand, the *I-V* linearity index is changed only slightly by fluorination (Table 2). This suggests that the translocation barrier is not as significant for transport in GMO bilayers. In DPhPC bilayers, the sublinear-to-superlinear transition occurs at a lower bath ion concentration in gA than in FgA, further indicating that the rate-limiting central barrier has been reduced by fluorination (Table 2). This is not as clear in GMO. The lack of effects in GMO are consistent with a lack of translocation limitation in the transport process. However, at very high concentrations (2 M), we expect entry to be less rate-limiting in GMO bilayers and translocation to become rate-limiting. Consistent with this expectation, the *I-V* becomes superlinear in this concentration range (Table 2), and the current ratio converts to values greater than 1.0, reaching a level of 1.1 in 2 M KCl (Fig. 6). This demonstrates that when the effects on translocation are measurable, fluorination enhances translocation in GMO as well.

TABLE 2 Linearity index

	NaCl		KCl	
Concentration (M)	gA	FgA	gA	FgA
In DPhPC/decane bilayers*				
0.1	0.92	0.83	0.88	0.75
0.2	1.00	0.88	0.88	0.92
0.5	1.20	1.03	1.42	0.96
1.0	1.21	1.15	1.30	1.14
2.0	1.40	1.18	1.52	1.29
In GMO/hexadecane bilayers*				
0.1	0.75	0.71	0.81	0.87
0.2	0.83	0.72	0.83	0.95
0.5	0.87	0.88	0.85	0.96
1.0	0.93	0.98	0.91	0.98
2.0	1.07	1.03	1.11	1.00

*Equation 4.

Conductance-concentration effects

Inferences about the changes in the binding affinity for ions in the channel can be made from the Eadie-Hofstee plot of zero-current conductance behavior. Eisenman et al. (1978) and Urban et al., (1980; see also Hladky and Haydon, 1984) have shown that the Eadie-Hofstee plot for gramicidin zero-current conductance (plotted against zero-current conductance divided by permeant ion activity) has three main regions. At intermediate values of the abscissa, the plot is linear with a negative slope, K_2, which for the two-site single file model is

$$K_2 = -2\frac{E}{D}\frac{K}{(K+E)} \tag{7}$$

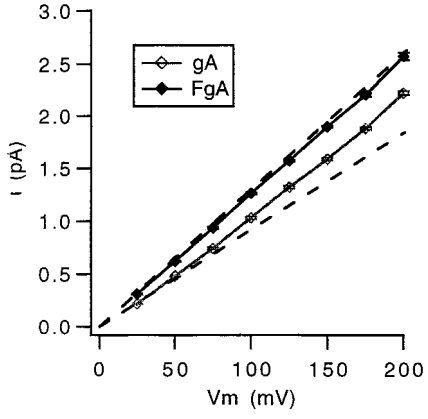

FIGURE 8 Exemplary current-voltage comparisons comparing gA to FgA in 0.5 M NaCl, using DPhPC bilayers. Dashed lines have slopes corresponding to the channel conductance at 25 mV and thus display deviations from *I-V* linearity. All currents are corrected to a nominal temperature of 23°C. Error bars represent ± SEM of *i*.

where K is the translocation rate constant, D is the rate constant for second ion entry, and E is the rate constant for second ion exit (Hladky and Haydon, 1984). It is evident that this slope, K_2, is inversely proportional to the second ion dissociation constant, E/D. At low values (high permeant ion activities) the data fall below the line because of self-block. At high values (low permeant ion activities), a foot in the plot can be seen for some ions (Cs^+, Rb^+, K^+) but not others (Na^+, Li^+) in GMO bilayers (Eisenman et al., 1978). The inverse of the slope in the foot region represents the first ion binding dissociation constant (Hladky and Haydon, 1984).

The Eadie-Hofstee plots of the 50-mV conductance in our data set (Fig. 9) are approximately linear with a drop on the left due to self-block. The activity range covered does not extend to low enough ion activities to demonstrate the single-occupancy foot. Comparison of native and fluorinated peptide slopes from lines least-squares fitted to the 0.1 M to 1 M data points shows that, for Na^+ and K^+ in DPhPC (Fig. 9 *a*) and K^+ GMO (*upper traces* in Fig. 9 *b*), K_2 is reduced by factors of 0.75–0.83 upon fluorination (see figure legend), consistent with destabilization of the ion binding relative to gA. For Na^+ in GMO (*lower traces* in Fig. 9 *b*), K_2 is essentially unchanged, being increased by a factor of 1.03.

Channel lifetimes

Channel lifetimes were not affected by fluorination for either GMO or DPhPC bilayers, as shown for 1 M KCl solutions in Table 3. The average lifetime in GMO/hexadecane bilayers (1.7 s) is greater than that in DPhPC/decane bilayers (0.5 s).

TABLE 3 Single-channel durations* (s) in DPhPC and GMO bilayers

	gA	FgA
DPhPC[#]	0.5 ± 0.02 (4)	0.5 ± 0.1 (4)
GMO[§]	1.7 ± 0.5 (5)	1.7 ± 0.4 (5)

*Mean ± interexperimental SD (n).
[#]All experiments carried out at 26.0 ± 1.5°C.
[§]All experiments carried out at 24.5 ± 1.0°C.

DISCUSSION

To summarize our data, Trp^{13} indole-5-fluorination apparently causes metal ion translocation to be enhanced, metal ion binding to be slightly destabilized, and proton entry and translocation to be inhibited in both DPhPC and GMO. The translocation enhancement in GMO bilayers becomes obvious at high ion concentrations (2 M KCl), where the FgA/gA current ratio reaches 1.1 and the I-V becomes superlinear. This is consistent with the observation that in DPhPC bilayers at 0.2 and 0.5 M salt concentrations, where the I-Vs become superlinear in that lipid, the FgA/gA current ratio is also ~1.1. Metal ion binding (except for Na^+ binding in GMO bilayer channels) is destabilized, judging from the Eadie-Hofstee plots. Proton conductance is inhibited by fluorination both at low H^+ concentrations (pH 2, where one would expect ion entry to be rate-limiting) and at high H^+ concentrations (pH 1, where translocation is expected to be rate-limiting; Akeson and Deamer, 1991).

Two hypotheses for the GMO anomaly

To explain the fact that fluorination does not increase conductance in GMO bilayers at all concentrations, we developed two hypotheses, which are illustrated in Fig. 10. A transport-kinetics hypothesis, the kinetic model, proposes that the fluorination-induced conductance increase is missing in GMO bilayers simply because the translocation barrier is not rate-limiting for gA in GMO bilayers. In fact, conductance is somewhat reduced at low concentrations because entry is rate-limiting and the positive end of the Trp^{13} dipole would be expected to inhibit entry. As an alternative hypothesis, termed the orientation model, it may be that fluorination causes a rotation of the average Trp position relative to the channel, such that the effect of the increased dipole is reduced or negated in GMO bilayers.

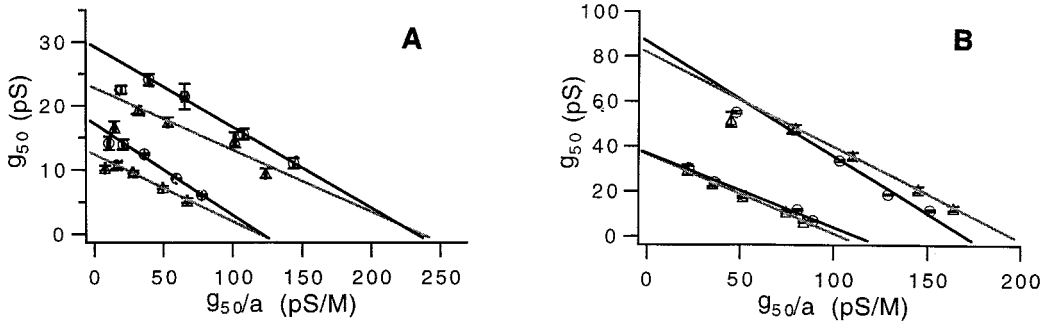

FIGURE 9 Eadie-Hofstee plot for KCl (*upper traces*) and NaCl (*lower traces*) in DPhPC bilayers (*A*) and GMO bilayers (*B*), comparing gA (△) to FgA (○). The darker lines are least-squares lines fitted to the FgA data, and the lighter lines are for gA data. Inverse slopes (K_2; see text), in units of M, were DPhPC, K^+: 0.10 (gA), 0.12 (FgA); Na^+: 0.12 (gA), 0.15 (FgA). For GMO they were K^+: 0.41 (gA), 0.51 (FgA); Na^+: 0.35 (gA), 0.34 (FgA). The y-intercept represents maximum conductance in the Michaelis-Menten approximation. Error bars represent ± SEM of i/V_m.

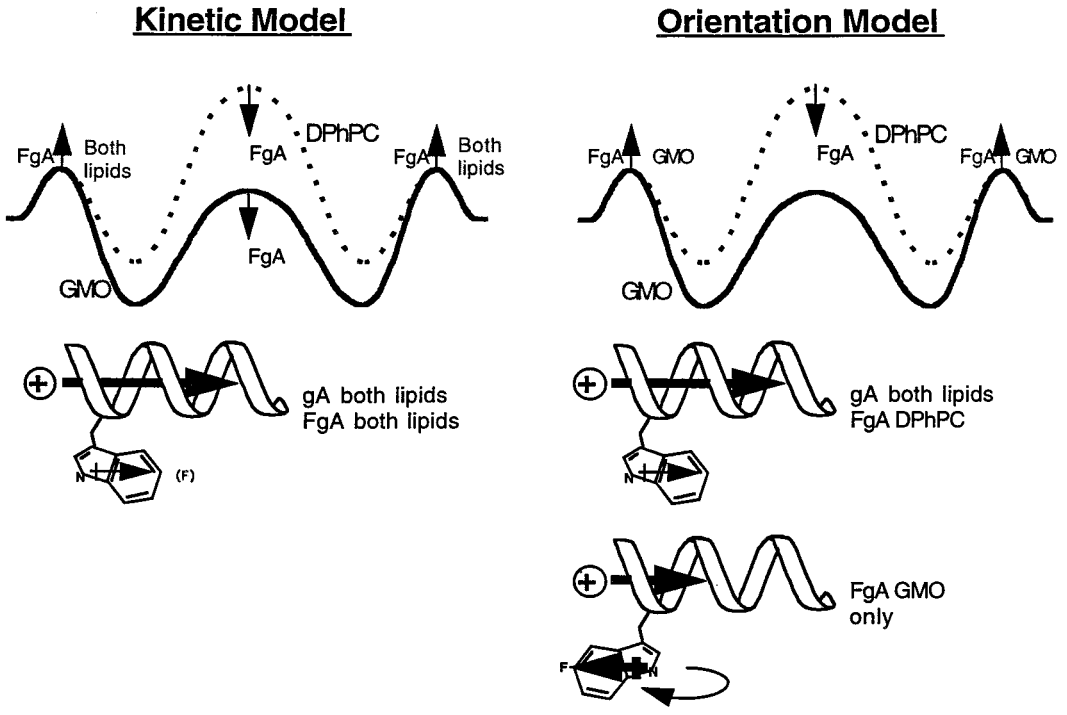

FIGURE 10 Two hypothetical models explaining the GMO anomaly are illustrated with free energy barrier profiles (*upper diagram*) and gA/FgA structure diagrams (*lower diagram*). The kinetic model on the left is based on the concept that translocation is not rate limiting in GMO, and therefore modulations of translocation are inconsequential. The orientation model on the right is based on the concept that the fluorinated Trp^{13} side chain undergoes a large (>60°) rotation in GMO bilayers but not in DPhPC bilayers and that the nonfluorinated side chain is similar to the solid-state NMR orientation in both types of bilayer, as expected from the diminished conductances observed with Trp-to-Phe replacement analogs of gA. In the energy profiles, the arrows denote the change in free energy expected upon fluorination of Trp^{13}. The dashed curve is for DPhPC bilayers, and the solid curve is for GMO. The structure models depict the left-hand monomer with the side chain of residue 13 only for simplicity. Ion flow direction and magnitude are symbolized by the arrow pointing from the ion into the channel. The increased dipole moment of the fluorinated side chain is represented by the heavier dipole arrow in the lower right-hand structure diagram, which represents the anomalous structure in the orientation model. The results appear to be sufficiently explained by the kinetic model and rule out the major orientation change of the anomalous structure.

Discrimination between these two models requires direct physical measurements of the Trp side-chain positions. However, a few additional qualitative arguments can be made from our data set.

Solid-state NMR results show that in dimyristoyl PC multilayers, 5-fluorination results only in a 2° change in orientation of the Trp^{13} side chain relative to the channel axis (Cotten and Cross, unpublished results), but this does not rule out an orientation change in a different lipid. However, for the orientation model to explain the GMO anomaly, a change in the rotameric state of the fluorinated side chain would be necessary, so that the axial component of the indole dipole is unchanged or reduced rather than enlarged. As mentioned above, the dipole moment of 5F-indole has been measured as 3.64 D in benzene, compared to 2.08 D for indole (Weiler-Feilchenfeld et al., 1970), an increase by a factor of 1.75. From position information derived from solid-state NMR with gramicidin embedded in DMPC multilayers (Hu and Cross, 1995), we estimate the angle of the Trp dipole with the channel axis to be 18° in the native gA channel. Although the angle of the dipole in the fluorinated indole relative to that of the nonfluorinated indole is not known, our ab initio computations (details to be presented elsewhere) indicate that it is not changed by more than a few degrees from that of indole. To negate a colinear enlargement of the indole dipole by a factor of 1.75, the angle with the axis would have to be increased to 57.6°, an increase of ~40°. An additional rotation of 72° in the same plane to a total of 90° would zero the axial moment, comparable to a Trp^{13}-Phe replacement, which has been shown to reduce conductance by a factor of 0.75 (in DPhPC bilayers with 1 M NaCl at $V_m = 200$ mV; Becker et al., 1991). These rotations of 40°-72° seem like reasonable bounds to the rotation needed for the orientation model to explain why in GMO fluorination anomalously decreases conductance by factors of ~0.85–1.0 (Fig. 6).

At least three lines of evidence contradict the orientation model. First, there was little change in the current ratios in monoglyceride bilayers over a large range of bilayer thicknesses. The hydrophobic region thicknesses range from the length of the channel, 25 Å in GMO/squalene, to nearly double the length at 48 Å for GMO/decane. One would expect this range of bilayer thicknesses to cause very different torques on the Trp^{13} side chain. The extent of the torque would depend on the contact angle between the lipid headgroups and the outer channel wall, which is unknown

(Nielsen et al., 1998, and references therein). Solvent-inflated bilayers all produce nearly the same conductance, suggesting dimpling. It is conceivable that the dimpling is quite broad, so that the contact angle does not differ much between the solvent-inflated bilayers. However, it is worth noting that in GME the gA and FgA conductances are greatly reduced (Table 1), which implies a significant perturbation of the lipid-peptide contact region, which surely would apply torque to the Trp^{13} side chain, yet the current ratio remains unchanged, indicating that the side-chain position is very stable.

Second, the fact that hydrogen conductance is reduced similarly for both types of bilayers suggests that fluorination does not cause a major side-chain orientation change. At low H^+ concentration and high voltage, one would expect entry to be rate-limiting, especially because Grotthus conductance is a very efficient mechanism for translocation in the channel. This is reflected to a certain extent in the *I-V* shapes for the two channels and two bilayer types in HCl at pH 2 (data not shown), which are linear to sublinear. If fluorination induced a 40–72° rotation in GMO bilayers, one would expect the current ratio in GMO bilayers to be different from that in DPhPC bilayers. Instead, they are both similarly reduced (0.78–0.85, excluding the 25-mV point for DPhPC; Fig. 7). One might counter that the low pH altered the conditions in the DPhPC bilayers such that a rotation was induced there as well. The control experiment in Fig. 7, where K^+ was made the dominant permeant ion while keeping the pH low, rules out this argument: the current ratio was dramatically altered, showing the GMO-DPhPC difference to be a specific feature of alkali metal cations.

Third, the slope in the Eadie-Hofstee plot for the fluorinated peptide is steeper by similar factors for K^+ in GMO and DPhPC and for Na^+ in DPhPC bilayers, suggesting that fluorination destabilized ion binding in the channel by a similar amount in the two lipids. This argues that the dipole orientation is similar in the two lipids. The lack of slope change for Na^+ in GMO may reflect a slight difference in Na^+ and K^+ binding sites in GMO bilayers. Electrostatic computations to be presented elsewhere indicate that, under the assumption that fluorination does not rotate the Trp^{13} side chain, the electric field change due to fluorination is stabilizing interior to the binding sites but is near zero or destabilizing at and exterior to the binding site, possibly explaining the Na^+/GMO result. In addition, individual Trp^{13} conformational changes are predicted to change the ion binding energy by >0.3 kcal/mol, which would produce a decrease in binding constant by a factor less than 0.6. The Eadie-Hofstee plot slopes should therefore be a very sensitive indicator of any side-chain rotations. The similarity between changes in K_2 for K^+ in the two lipids argues against a fluorination-induced rotation in GMO. Thus it appears from our measurements that the Trp^{13} indole position is quite robust, as we do not see evidence of large rotations upon fluorination, even though we have changed headgroup type and dramatically varied bilayer thickness. We do not feel it possible to distinguish 5–10° rotations (which might be expected to result from interactions with the interface, for instance) by these arguments, but we can comfortably rule out a 40–72° rotation.

The finding that fluorination has no effect on GMO channel lifetimes also suggests that there is no change in tryptophan-headgroup interactions. The most likely explanation for a fluorination-induced orientation shift would be the introduction of novel interactions between the tryptophan (fluorine) and the lipid headgroups, yet no change in lifetime is observed. However, although a few experiments indicate that Trp-lipid interactions affect channel lifetime (Becker et al., 1991; Seoh and Busath, 1995), there is currently no evidence that equal lifetimes imply equal conformations.

Kinetic model

The alternative proposal aimed at explaining the differences between the experimental outcomes of DPhPC and GMO is the kinetic model. This model presumes that differences in the kinetics of transport are directly responsible for the different behaviors in the two bilayers. Most of the basis of this hypothesis has already been described in the Results. Briefly, translocation is more rate-limiting in DPhPC than in GMO, judging from *I-V* shapes and self-block. Fluorination enhances alkali metal cation conductance, especially where translocation is rate-limiting, i.e., at high permeant ion concentrations and low voltages. It inhibits conductance in cases where entry is rate-limiting (low concentrations, high voltages). The permeant ion concentration at which the fluorination effect crosses over from inhibition to enhancement occurs in the same range as the cross-over from sublinear to superlinear *I-V*, consistent with this interpretation.

Interfacial dipole potential

The differences in the two lipids probably reflect differences in the interfacial dipole potentials (Hladky and Haydon, 1973; Haydon and Myers, 1973; Andersen and Fuchs, 1975; Pickar and Benz, 1978; Jordan, 1983; Jordan, 1984; Flewelling and Hubbell, 1986; Simon and McIntosh, 1989; Gawrisch et al., 1992; Brockman, 1994; Cseh and Benz, 1998). Although interfacial dipole potential effects have been traditionally expected to be modest, especially in comparison to surface charge effects, a few studies have drawn attention to similar differences in gramicidin conductance behavior in the two types of lipids and attributed them qualitatively to the dipole potential difference between the two bilayers (Eisenman et al., 1983; Akeson and Deamer, 1991).

Jordan's (1984) analysis of the dipole potential provides a method for estimating the penetration of the dipole field into the channel. However, it suffers from an unknown that has not yet been resolved, namely the structure of the lipid headgroups near the channel for bilayers thicker than the channel length of 25 Å. Jordan avoided the mathematical singularities and structural uncertainties about the putative "dimple" region near the channel by assuming, for the sake

of calculating the interfacial dipole potential penetration to the channel axis only, that the lipid pore surrounding the channel was a right cylinder, i.e., that there is no dimpling. Under this assumption, the computed "translocation barrier," defined as the energy difference between the binding site 2.5 Å into the channel and the channel center, does not differ between a 47-Å-thick PC bilayer and a 33-Å-thick GMO bilayer. Instead, the difference in interfacial dipole potential mainly causes a difference, relative to ion in bulk water, in the energy at the binding site.

Our linearity and self-block results suggest that the no-dimpling model for the lipid near the channel is incorrect. Furthermore, recent x-ray diffraction measurements of DMPC positions near densely packed gramicidin channels suggest that bilayer thickness is reduced in the presence of gramicidin to minimize hydrophobic mismatch (Harroun et al., 1998), as has always been assumed in traditional dimpling theories. However, our interpretations are based on the assumption that the interfacial dipole potential difference would modulate the translocation barrier significantly and therefore need to be considered cautiously until more information about the lipid structure near the channel entry is available.

Comparison to previous results

The possible role of the four Trps in gA in modulating channel conductance was identified in early analog (Bamberg et al., 1976), conformer, (Busath and Szabo, 1981), and UV-photolysis (Busath and Waldbillig, 1983) experiments. In all three cases, the Trp dipole was presumed to facilitate conductance in GMO bilayers. More recent studies of Trp replacement analogs have demonstrated that replacement of Trp side chains with four phenylalanines (Heitz et al., 1986) or two to four naphthylalanines (Daumas et al., 1989) reduces the conductance in GMO bilayers. The four Phe and three or four napthylalanine compounds have very superlinear *I-V*s (in contrast to gA and two-napthylalanine analogs), as though the translocation step is much more rate-limiting with these compounds.

An interesting attempt was made to control the dipole orientation, using two amino acids that represent a hybrid between napthylalanine and Trp. Both are expected to have dipole moments of a magnitude similar to that of Trp due to nitrogen (N) in the ring systems, but the locations of the N's differ. In L-3-(8-quinolyl)alanine the N is in the position homologous to that of indole; in L-3-(4-quinolyl)alanine it is on the other side of the ring system, so the dipole moment is oriented oppositely. Analogs with all four Trps replaced with the 8-quinolyl side chain had an approximately two- to fivefold conductance reduction. However, those with four 4-quinolyl side chains were further reduced (Daumas et al., 1991). This result is unexpected if the side chains are similarly oriented, because one analog should enhance conductance and the other reduce conductance. In Tyr replacement analogs with a series of increasingly hydrophobic protecting groups attached to the phenol O, conductance depends on hydrophobicity, suggesting that dipole orientation can be modulated by interactions between side chain and lipid (Benamar et al., 1993). These results illustrate the importance of knowing the precise orientation of the side chain.

Replacement of 1–3 Trps with Phes uniformly yielded conductance decrease factors of 0.14–0.74 in DPhPC bilayers (Becker et al., 1991; Fonseca et al., 1992). In particular, the conductance for Trp^{13}-Phe gA (1 M NaCl, 200 mV) is 11.2 pS compared to 15.0 pS for gA at 25°C (Becker et al., 1991). These can be compared to our measurements (under the same conditions but at 23°C) of 12.7 pS for gA and 15.6 pS for fluorinated Trp^{13} gA. (We note that there is a difference between the conductance for gA reported here and that reported by Becker et al. (1991). Sixty-three percent of the discrepancy between the two reports for gA is accounted for by the temperature difference, but the reason for the remaining discrepancy is uncertain. However, we note that our measurements at 100 mV, corrected to 25°C, are the same as the previous measurements of Russell et al. (1986): 12.3 pS at 100 mV, 25°C. Although our standard deviations would appear to preclude such a large discrepancy with the value of Becker et al. (1991), we suppose that the differences reflect variations in bilayer properties known to be common with lecithins, but apparently not fully manifested in our data set.) Thus the conductance increases by 3.8 pS upon the addition of one Trp dipole (2.08 D) at position 13 and another 2.9 pS upon fluorination of Trp^{13} (3.54 D). The conductance increase is therefore seen to be approximately proportional to the dipole moment.

However, this result may be viewed with skepticism because: 1) the conductance should be exponentially rather than linearly related to the energy/field (Hu and Cross, 1995); and 2) under some conditions, the rate-limiting step may be delocalized, as we believe is the case for GMO. For instance, the W13F gA conductance for 1 M KCl in GMO bilayers at 200 mV is 35–37 pS (Seoh and Busath, 1995), compared to 47–48 pS for gA, whereas in the measurements reported for K^+ here the conductance is decreased upon fluorination. Why did the addition of a Trp increase the conductance in GMO, whereas Trp fluorination causes a decrease? We argue qualitatively that the addition of the Trp^{13} dipole is productive, because without it translocation is still rate-limiting, but with it the rate-limiting barrier is delocalized or perhaps shifted to the entry step. In fact, the *I-V* for Trp^{13}-Phe gA in 1 M KCl is slightly superlinear, that of gA linear (Seoh and Busath, 1995), and that of fluorinated Trp^{13} gA (Table 2) slightly sublinear, consistent with this interpretation.

Analysis of uncertainty

The goal of directly correlating conductance modulation with side-chain position is yet to be realized. Although the fluorinated and native Trp side-chain positions have been measured in DMPC multilayers (Cotten and Cross, unpublished data), the conductance measurements reported here

have been limited to solvent-inflated bilayers, except for one set of experiments in GMO/squalene bilayers that are reasonably close to solvent-free. Experiments in folded DPhPC bilayers and DPhPC multilayers are under way to address this source of uncertainty. The data reported here argue against a large Trp dipole orientation change upon fluorination or a large difference in the native structure from the NH-out orientation obtained in other lipid bilayer environments, but small changes cannot be ruled out. In light of this fact, concern remains because of slight internal inconsistencies between our data and our interpretation. Why is the Eadie-Hofstee slope unchanged upon gA fluorination in GMO bilayers for Na^+? Why is the permeant ion concentration for transition from sublinear to superlinear *I-V* not better matched by the concentration at which the FgA/gA current ratio passes through 1? The increase in translocation barrier energy expected for DPhPC bilayers (compared to GMO bilayers) is relatively small, ~1.5 kcal/mol. Why is it so effective at changing *I-V* properties? Why is the conductance in GMO bilayers enhanced by addition of a Trp at position 13 but reduced by fluorination of Trp^{13}? All of these questions have been answered qualitatively, but quantitative analysis is needed to determine if the kinetic model is sufficient. Ideally, potentials derived from continuum theories or explicit atom theories combined with flux models can be used to fit the data (McGill and Schumaker, 1996) and should provide insights to these questions. Initial kinetic modeling is also expected to provide a simple preliminary approach.

SUMMARY

Fluorination of indole C-5 on the Trp^{13} side chain of gA has remarkably diverse consequences for channel properties, including increased Na^+ and K^+ conductance in DPhPC bilayers, decreased Na^+ and K^+ conductance in GMO bilayers (except in 2 M salt), decreased H^+ conductance in both bilayers, reduction of *I-V* linearity for Na^+ and K^+ in both bilayer types, and increase in Eadie-Hofstee K_2 slope (second ion binding destabilization) for Na^+ and K^+ in DPhPC and for K^+ in GMO. The diversity of effects does not appear to be due to fluorination-induced side-chain rotations because 1) current ratios remain similar in monoglyceride bilayers over a large range of bilayer thicknesses; 2) hydronium conductances at pH 2, where entry is thought to be rate-limiting, are similar in the two lipids; and 3) Eadie-Hofstee plots indicate similar degrees of destabilization for K^+ in both types of lipids (which is expected to be especially sensitive to side-chain conformation). We propose that the GMO anomaly is due to a reduced interfacial dipole potential.

Note added in proof: The effect of transmembrane peptides on lipid bilayer thickness has recently been demonstrated by de Planque et al. (1998).

We thank Crystal Budge, David Lloyd, James Howard, James Ricks, Shawn Crook, and Vivek Ramakrishnan for helping to perform some of the experiments reported here, and Olaf Andersen and Eric Jakobsson for advice.

This project was supported by National Institutes of Health Grant R01 AI23007 to TAC and DDB.

REFERENCES

Akeson, M., and D. W. Deamer. 1991. Proton conductance by the gramicidin water wire. Model for proton conductance in the F_1F_0 ATPases? *Biophys. J.* 60:101–109.

Andersen, O. S. 1983. Ion movement through gramicidin A channels. Interfacial polarization effects on single-channel current measurements. *Biophys. J.* 41:135–146.

Andersen, O. S., and M. Fuchs. 1975. Potential energy barriers to ion transport within lipid bilayers. Studies with tetraphenylborate. *Biophys. J.* 15:795–830.

Andersen, O. S., D. V. Greathouse, L. L. Providence, M. D. Becker, and R. E. Koeppe, II. 1998. Importance of tryptophan dipoles for protein function: 5-fluorination of tryptophans in gramicidin A channels. *J. Am. Chem. Soc.* 120:5142–5146.

Andersen, O. S., and R. E. Koeppe, II. 1992. Molecular determinants of channel function. *Physiol. Rev.* 72:S89–S158.

Bamberg, E., K. Noda, E. Gross, P. Läuger. 1976. Single-channel parameters of gramicidin A, B, and C. *Biochim. Biophys. Acta.* 419:223–228.

Becker, M. D., D. V. Greathouse, R. E. Koeppe, II, and O. S. Andersen. 1991. Amino acid sequence modulation of gramicidin channel function: effects of tryptophan-to-phenylalanine substitutions on the single-channel conductance and duration. *Biochemistry.* 30:8830–8839.

Benamar, D., P. Daumas, Y. Trudelle, B. Calas, R. Bennes, and F. Heitz. 1993. Influence of the nature of the aromatic side-chain on the conductance of the channel of linear gramicidin: study of a series of 9,11,13,15-Tyr(O-protected) derivatives. *Eur. Biophys. J.* 22:145–150.

Bevington, P. R. 1969. Data Reduction and Error Analysis for the Physical Sciences. McGraw-Hill, New York.

Branden, C., and J. Tooze. 1991. Introduction to Protein Structure. Garland Publishing, New York and London.

Brockman, H. 1994. Dipole potentials of lipid membranes. *Chem. Phys. Lipids.* 73:57–79.

Busath, D. D. 1993. The use of physical methods in determining gramicidin channel structure and function. *Annu. Rev. Physiol.* 55:473–501.

Busath, D., and G. Szabo. 1981. Gramicidin forms multi-state rectifying channels. *Nature.* 294:371–373.

Busath, D., and G. Szabo. 1988. Low conductance gramicidin A channels are head-to-head dimers of $\beta^{6.3}$-helices. *Biophys. J.* 53:689–695.

Busath, D. D., and R. C. Waldbillig. 1983. Photolysis of gramicidin A channels in lipid bilayers. *Biochim. Biophys. Acta.* 736:28–38.

Cseh, R., and R. Benz. 1998. The absorption of phloretin to lipid monolayers and bilayers cannot be explained by Langmuir adsorption isotherms alone. *Biophys. J.* 74:1399–1408.

Daumas, P., D. Benamar, F. Heitz, L. Ranjalahy-Rasoloarijao, R. Mouden, R. Lazaro, and A. Pullman. 1991. How can the aromatic side chains modulate the conductance of the gramicidin channel? A new approach using non-coded amino acids. *Int. J. Pept. Protein Res.* 38:218–228.

Daumas, P., F. Heitz, L. Ranjalahy-Rasoloarijao, and R. Lazaro. 1989. Gramicidin A analogs: influence of the substitution of the tryptophans by naphthylalanines. *Biochimie.* 71:77–81.

de Planque, M. R. R., D. V. Greathouse, R. E. Koeppe II, H. Schäfer, D. Marsh, and J. A. Killian. 1998. Influence of lipid/peptide hydrophobic mismatch on the thickness of diacylphosphatidyl-chlorine bilayers. A ^2H NMR and ESR study using designed transmembrane α-helical peptides and gramicidin A. *Biochemistry*. 37:9333–9345.

Dilger, J. P. 1981. The thickness of monoolein lipid bilayers as determined from reflectance measurements. *Biochim. Biophys. Acta.* 645:357–363.

Doyle, D. A., J. M. Cabral, R. A. Pfuetzner, A. Kuo, J. M. Gulbis, S. L. Cohem, B. T. Chait, and R. MacKinnon. 1998. The structure of the potassium channel: molecular basis of K^+ conduction and selectivity. *Science.* 280:69–77.

Eisenman, G., J. Sandblom, and J. Hägglund. 1983. Electrical behavior of single-filing channels. *In* Structure and Function in Excitable Cells. W.

Chang, I. Tasaki, W. Adelman, and R. Leuchtag, editors. Plenum, New York. 383–413.

Eisenman, G., J. Sandblom, and E. Neher. 1978. Interactions in cation permeation through the gramicidin channel. Cs^+, Rb^+, K^+, Na^+, Li^+, Tl^+, H^+, and effects of anion binding. *Biophys. J.* 22:307–340.

Fields, C. G., G. B. Fields, R. L. Noble, and T. A. Cross. 1989. Solid phase peptide synthesis of ^{15}N-gramicidins A, B, and C and high performance liquid chromatographic purification. *Int. J. Pept. Protein Res.* 33: 298–303.

Fields, G. B., C. G. Fields, J. Petefish, H. E. Van Wart, and T. A. Cross. 1988. Solid-phase peptide synthesis and solid-state NMR spectroscopy of [Ala^3-^{15}N][Val^1]gramicidin A. *Proc. Natl. Acad. Sci. USA.* 85: 1384–1388.

Flewelling, R. F., and W. L. Hubbell. 1986. The membrane dipole potential in a total membrane potential model. Applications to hydrophobic ion interactions with membranes. *Biophys. J.* 49:541–552.

Fonseca, V., P. Daumas, L. Ranjalahy-Rasoloarijao, F. Heitz, R. Lazaro, Y. Trudelle, and O. S. Andersen. 1992. Gramicidin channels that have no tryptophan residues. *Biochemistry.* 31:5340–5350.

Gawrisch, K., D. Ruston, J. Zimmerberg, V. A. Parsegian, R. P. Rand, and N. Fuller. 1992. Membrane dipole potentials, hydration forces, and the ordering of water at membrane surfaces. *Biophys. J.* 61:1213–1223.

Hägglund, J. V., G. Eisenman, and J. P. Sandblom. 1984. Single-salt behavior of a symmetrical 4-site channel with barriers at its middle and ends. *Bull. Math. Biol.* 46:41–80.

Harroun, T. A., K. He, W. T. Heller, T. M. Weiss, and H. W. Huang. 1998. Direct observation of membrane mediated peptide-peptide interactions with x-ray scattering. *Biophys. J.* 74:A302.

Haydon, D. A., and V. B. Myers. 1973. Surface charge, surface dipoles and membrane conductance. *Biochim. Biophys. Acta.* 307:429–443.

Heinemann, S. H., and F. J. Sigworth. 1989. Estimation of Na^+ dwell time in the gramicidin A channel. Na^+ ions as blockers of H^+ currents. *Biochim. Biophys. Acta.* 987:8–14.

Heitz, F., P. Daumas, N. Van Mau, R. Lazaro, Y. Trudelle, C. Etchebest, and A. Pullman. 1988. Linear gramicidins: influence of the nature of the aromatic side chains on the channel conductance. *In* Transport Through Membranes: Carriers, Channels, and Pumps. A. Pullman, J. Jortner, and B. Pullman, editors. Kluwer Academic, Dordrecht, Boston, and London. 147–165.

Heitz, F., C. Gavach, G. Spach, and Y. Trudelle. 1986. Analysis of the ion transfer through the channel of 9,11,13,15-phenylalanylgramicidin A. *Biophys. Chem.* 24:143–148.

Heitz, F., G. Spach, and Y. Trudelle. 1982. Single channels of 9, 11, 13, and 15-destryptophyl-phenylalanyl-gramicidin A. *Biophys. J.* 40:87–89.

Heitz, F., N. Van Mau, R. Bennes, P. Daumas, and Y. Trudelle. 1989. Single channels and surface potentials of linear gramicidins. *Biochimie.* 71:83–88.

Hille, B. 1992. Ionic Channels of Excitable Membranes, 2nd Ed. Sinauer Associates, Sunderland, MA.

Hille, B., and W. Schwarz. 1978. Potassium channels as multi-ion single-file pores. *J. Gen. Physiol.* 72:409–442.

Hladky, S. B., and D. A. Haydon. 1972. Ion transfer across lipid membranes in the presence of gramicidin A. I. Studies of the unit conductance channel. *Biochim. Biophys. Acta.* 274:294–312.

Hladky, S. B., and D. A. Haydon. 1973. Membrane conductance and surface potential. *Biochim. Biophys. Acta.* 318:464–468.

Hladsky, S. B. and D. A. Haydon. 1984. Ion movements in gramicidin channels. *Curr. Topics Membrane Transport.* 21:327–372.

Hu, W., and T. A. Cross. 1995. Tryptophan hydrogen bonding and electrical dipole moments: functional roles in the gramicidin channel and implications for membrane proteins. *Biochemistry.* 34:14147–55.

Hu, W., N. D. Lazo, and T. A. Cross. 1995. Tryptophan dynamics and structural refinement in a lipid bilayer environment: solid state NMR of the gramicidin channel. *Biochemistry.* 34:14138–14146.

Hu, W., K.-C. Lee, and T. A. Cross. 1993. Tryptophans in membrane proteins: indole ring orientations in the gramicidin channel. *Biochemistry.* 32:7035–7047.

Jordan, P. C. 1983. Electrostatic modeling of ion pores. II. Effects attributable to the membrane dipole potential. *Biophys. J.* 41:189–195.

Jordan, P. C. 1984. The total electrostatic potential in a gramicidin channel. *J. Membr. Biol.* 78:91–102.

Ketchem, R. R., B. Roux, and T. A. Cross. 1997. High-resolution polypeptide structure in a lamellar phase lipid environment from solid state NMR derived orientational constraints. *Structure.* 5:1655–1669.

Killian, J. A., K. N. J. Burger, and B. De Kruijff. 1987. Phase separation and hexagonal HII phase formation by gramicidins A, B, and C in dioleoylphasphatidylcholine model membranes. A study on the role of the tryptophan residues. *Biochim. Biophys. Acta.* 897:269–284.

Koeppe, R. E., II, J. A. Killian, and D. V. Greathouse. 1994. Orientations of the tryptophan 9 and 11 side chains of the gramicidin channel based on deuterium nuclear magnetic resonance spectroscopy. *Biophys. J.* 66:14–24.

Koeppe, R. E., J. L. Mazet, and O. S. Andersen. 1990. Distinction between dipolar and inductive effects in modulating the conductance of gramicidin channels. *Biochemistry.* 29:512–520.

Koeppe, R. E., II, and L. B. Weiss. 1981. Resolution of linear gramicidins by preparative reversed-phase high-performance liquid chromatography. *J. Chromatogr.* 208:414–418.

Lazo, N. D., and D. T. Downing. 1998. Amyloid fibrils may be assembled from β-helical protofibrils. *Biochemistry.* 37:1731–1735.

Marsh, D. 1990. CRC Handbook of Lipid Bilayers. CRC Press, Boca Raton, FL.

Martínez, G., and M. Sancho. 1993. Electrostatic interactions in gramicidin channels—3-dielectric model. *Eur. Biophys. J.* 22:301–307.

McGill, P., and M. F. Schumaker. 1996. Boundary conditions for single-ion diffusion. *Biophys. J.* 71:1723–1742.

Moore, W. J. 1972. Physical Chemistry. Prentice-Hall, Englewood Cliffs, NJ.

Nielsen, C., M. Goulian, and O. S. Andersen. 1998. Energetics of inclusion-induced bilayer deformations. *Biophys. J.* 74:1966–1983.

Partenskii, M. B., M. Cai, and P. C. Jordan. 1991. A dipolar chain model for the electrostatics of transmembrane ion channels. *Chem. Phys.* 153: 125–131.

Pickar, A. D., and R. Benz. 1978. Transport of oppositely charged lipophilic probe ions in lipid bilayer membranes having various structures. *J. Membr. Biol.* 44:353–376.

Roeske, R. W., T. P. Hrinyo-Pavlina, R. S. Pottorf, T. Bridal, X.-Z. Jin, and D. Busath. 1989. Synthesis and channel properties of [tau^{16}]gramicidin A. *Biochim. Biophys. Acta.* 982:223–227.

Roux, B., and M. Karplus. 1993. Ion transport in a model gramicidin channel. Free energy of the solvated right-handed dimer in a model membrane. *J. Am. Chem. Soc.* 115:3250–3262.

Russell, E. W. B., L. B. Weiss, F. I. Navetta, R. E. Koeppe, II, and O. S. Andersen. 1986. Single-channel studies on linear gramicidin with altered amino acid side chains. *Biophys. J.* 49:673–686.

Sancho, M., and G. Martínez. 1991. Electrostatic modeling of dipole-ion interactions in gramicidin like channels. *Biophys. J.* 60:81–88.

Sandblom, J. P., R. M. Josefsson, and T. Larsson. 1990. Some properties of channels formed by gramicidin A and B, including their hybrid forms, in the presence of protons. *In* 10th International Biophysics Congress, Abstracts. 391.

Seoh, S., and D. Busath. 1995. Gramicidin tryptophans mediate formamidinium-induced channel stabilization. *Biophys. J.* 68:2271–2279.

Simon, S. A., and T. J. McIntosh. 1989. Magnitude of solvation pressure depends on dipole potential. *Proc. Natl. Acad. Sci. USA.* 86:9263–9267.

Takeuchi, H., Y. Nemoto, and I. Harada. 1990. Environments and conformations of tryptophan side chains of gramicidin A in phospholipid bilayers studied by Raman spectroscopy. *Biochemistry.* 29:1572–1579.

Thulin, C., R. Hendershot, C. Cole, R. Phillips, N. Bingham, V. Ramakrishnan, D. Anderson, M. Cotten, T. Cross, and D. D. Busath. 1998. 5-Fluorination of Trp-13 in gramicidin A can increase (lecithin) or decrease (monoolein) channel conductance. *Biophys. J.* 74:A232.

Urban, B. W., S. B. Hladky, and D. A. Haydon. 1978. The kinetics of ion movements in the gramicidin channel. *Fed. Proc.* 37:2628–2632.

Urban, B. W., S. B. Hladky, and D. A. Haydon. 1980. Ion movements in gramicidin pores. An example of single-file transport. *Biochim. Biophys. Acta.* 602:331–354.

Venkatachalam, C. M., and D. W. Urry. 1983. Theoretical conformational analysis of the gramicidin A transmembrane channel. I. Helix sense and energetics of head-to-head dimerization. *J. Comp. Chem.* 4:461–469.

Waldbillig, R. C., and G. Szabo. 1979. Planar bilayer membranes from pure lipids. *Biochim. Biophys. Acta.* 557:295–305.

Weiler-Feilchenfeld, H., A. Pullman, H. Berthod, and C. Giessner-Prettre. 1970. Experimental and quantum mechanical studies of the dipole moments of quinoline and indole. *J. Mol. Struct.* 6:297–304.

Woolf, T. B., and B. Roux. 1997. The binding site of sodium in the gramicidin A channel: comparison of molecular dynamics with solid-state NMR data. *Biophys. J.* 72:1930–1945.

Woolley, G. A., and B. A. Wallace. 1992. Model ion channels—gramicidin and alamethicin. *J. Membr. Biol.* 129:109–136.

Yoder, M. D., S. E. Lietzke, and F. Jurnak. 1993. Unusual structural features in the parallel beta-helix in pectate lyases. *Structure.* 15: 241–251.